EUROFUSION WPMAT-PR(15) 12890

L Malerba et al.

Effect of Cr content on the nanostructural evolution of irradiated ferritic/martensitic alloys: an object kinetic Monte Carlo model

Preprint of Paper to be submitted for publication in
Journal of Nuclear Materials

This work has been carried out within the framework of the EUROfusion Consortium and has received funding from the Euratom research and training programme 2014-2018 under grant agreement No 633053. The views and opinions expressed herein do not necessarily reflect those of the European Commission.

Effect of Cr content on the nanostructural evolution of irradiated ferritic/martensitic alloys: an object kinetic Monte Carlo model

M. Chiapetto [a,b,1], L. Malerba [a], C.S. Becquart [b]

[a] *SCK•CEN, Nuclear Materials Science Institute, Boeretang 200, B-2400 Mol, Belgium*

[b] *Unité Matériaux Et Transformations (UMET), UMR 8207, Université de Lille 1, ENSCL, F-59600 Villeneuve d'Ascq Cedex, France*

ABSTRACT

Self-interstitial clusters diffusivity in Fe-Cr alloys, model materials for high-Cr ferritic/martensitic steels, is known to be reduced in a non-monotonic way as a function of Cr concentration: it first decreases, then increases. This non-monotonic behaviour is caused by a relatively long-ranged attractive interaction between Cr atoms and crowdions and correlates well with the experimentally observed swelling in these alloys under neutron irradiation, also seen to first decrease and then increase with increasing Cr content, under comparable irradiation conditions. The mobility of one-dimensional migrating clusters is considered key to determine swelling susceptibility: the faster they diffuse to sink with respect to vacancies, the higher the swelling. Thus, the mentioned correlation makes physical sense. However, no model has ever been developed that quantitatively proves the validity of this correlation. In this work we developed physically-based sets of parameters for object kinetic Monte Carlo (OKMC) simulations intended to study the nanostructure evolution under irradiation in Fe-Cr-C alloys, with the idea of verifying the existence of such correlation. The nanostructural evolution in four Fe-Cr-C alloys (containing 2.5, 5, 9 and 12 wt.% Cr) neutron irradiated up to ~0.6 dpa at 563 K was simulated according to the model. It could be thereby proven that the major influence of Cr on the nanostructural evolution was the suppression of vacancy clustering, when compared to pure Fe, as a consequence of the reduced mobility of self-interstitial clusters and subsequent enhanced recombination with vacancies. This provides a clear framework to interpret the non-monotonic dependence of swelling in Fe-Cr alloys versus Cr content. In addition, our model suggests that the amount of C in the matrix has also an important role: high amounts of it may counteract the beneficial effect that Cr has in reducing swelling.

1. Introduction

High-Cr ferritic/martensitic (F/M) steels are candidate structural materials in the breeding blanket of future fusion reactors [1], as well as for fuel cladding and other core components in GenIV reactors [2,3]. The Cr content in these steels is known to have a strong effect on radiation defect stability and, in general, on the properties of the material. For this reason, Fe-Cr alloys are often employed as model materials in irradiation experiments and subsequent characterization [4-20]. It is known in particular from these studies that the addition of Cr to Fe reduces radiation-induced swelling, typically by an order of magnitude [4, 6-9]. Specifically, swelling drastically decreases already with the addition of small quantities of Cr (few wt.%), remains low between ~1-10 %Cr and then rises again, although

1

Corresponding author. *Tel.*: +32 (0)14 33 31 81.

E-mail address: mchiapet@sckcen.be.

the actual behaviour and thresholds depend strongly on the irradiation conditions and swelling local maxima already around 9 %Cr are observed at very high irradiation dose [4-9]. Cr content is therefore a key parameter, the effect of which needs to be fully understood in order to guarantee the best swelling resistance, together with minimum embrittlement, and cope with the high energy neutron dose in the harsh environmental conditions expected in future nuclear systems. With this aim, international efforts are being made to develop physically-based models capable of describing the behaviour of Fe-Cr alloys under irradiation as a function of irradiation parameters (fluence, temperature, …) and Cr content [21-30].

Both experimental [11-14] and theoretical [26-30] studies, the latter making use of atomistic computer simulation techniques, suggest that one of the main effects of Cr on the nanostructural evolution under irradiation of Fe-Cr alloys is the reduction of the mobility of self-interstitial clusters (dislocation loops) and their stabilization versus temperature, especially for ½⟨111⟩ loops [16]. This mobility reduction, physically due to the attractive interaction between the Cr atoms dispersed in the solid solution and the crowdions that form the clusters, has been theoretically shown to exhibit the same non-monotonic dependence on Cr content as empirically observed in void swelling suppression (cfr. [4, 6-8] and [27-30]). However, up to now the connection between slowing down/stabilization of interstitials clusters due to Cr in Fe and swelling suppression in Fe-Cr alloys as compared to Fe has been argued, but not fully demonstrated. In particular, no suitable model capable of reproducing the effect of irradiation at the correct scale and up to a relevant dose has been applied, yet, to show this connection. In this work we develop and apply a model of this type to simulate the nanostructural evolution in Fe-Cr-C alloys with different Cr content, neutron-irradiated at ~290°C up to doses of the order of ~1 dpa. This was possible by using as starting point a model recently developed for Fe-C alloys [31, 32]. More in detail, we investigate here Fe alloys with four Cr concentrations (2.5, 5, 9 and 12 wt.%Cr, nominal compositions), by simulating their neutron irradiation up to ~0.6 dpa at 563 K. The results are compared with those stemming from the thorough microstructural examination of these alloys, that was completed over the past years [9, 10, 15-19, 33]. As there is no single experimental technique capable of giving a complete description of the irradiation-induced microstructure of steels and Fe-based model alloys, a combination of techniques sensitive to defects at the nm-scale, such as transmission electron microscopy (TEM) [10, 16], atom probe tomography (APT) [19], small angle neutron scattering (SANS) [17, 18] and positron annihilation spectroscopy (PAS) [9], was used in order to thoroughly characterize the binary Fe-Cr alloys in terms of defect densities and average sizes of both vacancy and SIA cluster populations at different doses. With our model we show that, indeed, the effect of Cr on the interstitial clusters properties is dominant to explain the nanostructure evolution observed in these alloys under irradiation; we also reveal the importance of the actual amount of C in the matrix to determine the evolution of the populations of loops and voids.

The paper is organized as follows: the simulation method is presented in section 2, while section 3 outlines the main aspects of the adopted parameterization, together with the influence of Cr content on the mobility of the interstitial cluster population. In section 4 we show the simulation results, in terms of evolution of both vacancy and interstitial defect populations: they are compared with the corresponding experimental observations, as well as with the results predicted under the same conditions by the already developed Fe-C model. Finally, sections 5 and 6 contain, respectively, a discussion of the results and our conclusions.

2. Computation method

For the simulation of the nanostructural evolution under irradiation of the investigated Fe-Cr-C model alloys we use the object kinetic Monte Carlo (OKMC) code LAKIMOCA, thoroughly described in [34]. The approach we adopt is explained in detail in [31, 32]. For convenience, we highlight here the fundamental ideas. The OKMC is a stochastic method used to describe the evolution of defects and their clusters in materials subjected to irradiation and/or annealing, disregarding the detail of processes directly involving atoms and focusing instead only on the properties of defects, treated as objects. Irradiation produces point-defects, namely vacancies (V) and self-interstitial atoms (SIA),

which may form clusters. These clusters accumulate in growing number densities and size and may also form complexes with specific solute atoms, if present. The objects we consider are therefore V and SIA clusters or any other nanostructural feature, like carbon (C) atoms or carbon-vacancy (C_mV_n) complexes, located in a simulation volume in which the object coordinates are known and tracked. It is, however, important to note that, in the case of Fe-Cr alloys addressed here, Cr atoms are not treated as objects, because this would lead to an unnecessarily large number of elements in the system that would slow down enormously the simulation. Instead, the effect of Cr is introduced assuming that it changes the properties of the objects, i.e. applying a "grey alloy" approach.
Each of the objects introduced in the system can undergo events such as migration, recombination, or clustering of defects, which take place in the simulation volume (or box) according to pre-defined probabilities. Every object has an associated reaction volume, that is generally a sphere, with the exception of large dislocation loops (> 150 SIA), which are represented by toroids. When the reaction volumes of two objects overlap, a predefined reaction, like clustering between two vacancy clusters, or annihilation between a vacancy and an SIA, takes place. The events in the OKMC simulation determine the dynamics of the system. The probability for the objects to perform an event are given in terms of Arrhenius frequencies for thermally activated processes:

$$\Gamma_i = \nu_i exp\left(\frac{-A_i}{k_B T}\right) \quad (1)$$

Here ν_i is the attempt frequency (alias the prefactor) of the event i; A_i is the corresponding activation energy, which must embody both the thermodynamics and the kinetics of the system being studied; k_B is the Boltzmann's constant and T is the irradiation temperature expressed in K. Given that the activation energy for migration or emission depends on type and size of the objects, a very large number of parameters is needed for a standard simulation. For every simulation step an event is chosen, based on the corresponding probabilities in the parameterization and according to the stochastic Monte Carlo algorithm [35]. The simulated time is increased following the residence time algorithm [36, 37]:

$$\Delta t = \frac{-lnR}{\sum_1^N \Gamma_i} \quad (2)$$

where the time increase is obtained as inverse of the sum of all the frequencies Γ_i associated with each of the N possible events, while R is a uniform random number between 0 and 1, included to take into account correctly the stochasticity, according to the Poisson distribution.

A special kind of objects employed in our model are traps and sinks. These are immobile spherical objects that can, respectively, trap mobile defects (vacancy and SIA clusters) with a certain binding energy, E_t^δ, that depends on the size and type of the trapped object, or remove them from the system. Traps are used to simulate the effect of carbon or carbon-vacancy complexes (in our case C_2V, see [31]) that are known to be able to trap defect clusters. Sinks have the role that dislocations have in the material: their radius and number are defined in such a way that their sink strength equals the sink strength of the corresponding material dislocation density [38]. However, SIA clusters are often observed by transmission electron microscopy to decorate dislocations in the materials of interest here [16, 33, 39], meaning that they are not absorbed if large enough. We therefore only allow clusters smaller than the core of the dislocations, i.e. size 1-4, to be absorbed by the sinks. The radius of interaction of traps with defects, R_s^δ, has to be specified and changes between vacancy and SIA clusters:

$$R_s^\delta = \frac{\rho B}{4\pi N_s} Z^\delta - r_1^\delta \quad (3)$$

Here δ = *{V; SIA}* denote parameters for vacancies and SIA, respectively. B is the volume of the simulation box and N_s is the number of sinks. Since the theoretical sink strength expressions were derived for point-like defects, in Eq. (3) the single-defect radius, r_1^δ, is subtracted from the sink radius.

More specifically, we have a capture radius of r_1^V = 0.432 nm for a single vacancy and r_1^{SIA} = 0.517 nm for a single SIA. The bias factor, Z^δ, takes into account the strain field of the different defects and since the strain field of SIA is larger than that of vacancies, Z^V = 1.0 was assumed, while Z^{SIA} was adjusted, finding eventually that 1.6 was a suitable value. The absorption of defects at grain boundaries, on the other hand, was taken into account by applying the algorithm described in [40]: each object has both coordinates expressing its position in the simulation box, subjected to periodic boundary conditions, and coordinates expressing its distance from the centre of a supposedly spherical grain, which are not subjected to periodicity. When the latter distance happens to correspond to the grain radius, the objects disappears, irrespective of its position inside the box.

LAKIMOCA can simulate damage production from electron, ion and neutron irradiation. When simulating neutron irradiation, debris of vacancy and SIA objects of different sizes are randomly introduced in the system at a certain rate per unit time and volume, corresponding to a certain dpa rate. The cascade defect populations are chosen randomly from a database [41-43] of displacement cascades that were simulated using molecular dynamics (MD) with energies of 5 keV, 10 keV, 20 keV, 30 keV, 40 keV, 50 keV and 100 keV. The accumulated dpa is calculated using the NRT expression for the number of displacements, n_d, in each cascade, given its energy E_{MD} [44]:

$$n_d = \frac{0.8E_{MD}}{2E_D} \tag{4}$$

E_{MD} should actually be the damage energy, i.e. the fraction of the kinetic energy of the primary knock-on atom (PKA) spectrum that is not absorbed by electronic excitation, which is well approximated by the energy of the cascades in the MD simulations, that do not take into account the effect of electrons. The displacement threshold energy for Fe is E_D = 40 eV.

3. Model parameterization and simulation conditions

Most parameters in the model are exactly the same as in the Fe-C model described in [31, 32]. Here we detail only those that differ. The effect of Cr was introduced assuming that its effect was to change the mobility and stability of SIA type defects; thus, the main differences in the parameters with respect to [31, 32] concern this class of defects. The properties of vacancy type defects, in contrast, are assumed not to be influenced by Cr: this is justified because several experimental and theoretical studies have revealed that Cr atoms in Fe interact only very weakly with vacancies, with hardly any influence on their stability and mobility (see discussion in [21]; see also [45, 46]). Thus, all parameters for vacancies are exactly the same as in [31].

The reduction of the SIA cluster mobility in a given Fe-Cr alloy can be expressed, for a given cluster of size n, in terms of ratio between the diffusion coefficients in the alloy and in pure Fe, $r = D_n^{FeCr}/D_n^{Fe}$ [27]. Values for these ratios were calculated at 600 K atomistically, employing different methods, in [27-30] for a discrete number of ½⟨111⟩ cluster sizes, up to 331 SIA. Here we interpolated these data points (see Fig. 1), as taken from [28], for intermediate sizes and different Cr contents, using cubic splines (given in Table 1); then, the values corresponding to the concentrations of interest were used to tune (i.e. multiply) the SIA cluster attempt frequencies for migration as a function of cluster size, n^{SIA} (number of SIA), that was adopted in [31] for Fe-C alloys. In other words, in Fe-C the prefactors for clusters of sizes ≥ 7 SIA were estimated using the following expression:

$$\nu_{Fe-C} = \frac{c}{\left(n^{SIA}\right)^{0.8}} \tag{5}$$

where the constant c took the value 8.11×10^{12}. In Fe-Cr-C we used $\nu_{Fe-Cr} = r(\%Cr, n^{SIA})\times\nu_{Fe-C}$, where $r(\%Cr,n^{SIA})$ is given in Table 1. Note that the exponent of n^{SIA} in the denominator can theoretically vary between 0.5 (independent crowdion model) [47] and 1 (migration via kink pair formation along the edge of a loop) [48]: the value 0.8 adopted in [31, 32] respects the theory and

corresponds to the value determined experimentally by Arakawa et al. [49]. The original prefactors for clusters of sizes $\leq$ 10 SIA, as calculated in [31], are reported in Table 2, together with the tuned attempt frequencies for all investigated Fe-Cr-C alloys. For clusters of sizes > 331 SIA, in the absence of data, a constant reduction in the SIA attempt frequency was assumed, equal to the one estimated for SIA clusters containing 331 defects. The hidden hypothesis here is that we are implicitly assuming Cr atoms to be *constantly* randomly distributed in the system, i.e. the model cannot treat processes such as precipitation or segregation. Since Cr will redistribute under irradiation, this represents an approximation for our model. However, neglecting Cr precipitation is correct for all alloys except 12 %Cr, where alpha prime precipitation occurs. Also neglecting Cr segregation, on the other hand, is roughly correct, with the exception of the potential effect of Cr segregation on loops, as discussed in section 4.3.

Other differences in the simulation conditions of the Fe-Cr-C alloys come from the fact that the initial microstructure of the materials before irradiation was known from the experimental characterisation to be different with respect to Fe-C. With the increase of Cr content, the microstructure of the reference Fe-Cr-C model alloys is known experimentally to vary progressively from ferrite (2.5%) to tempered martensite (5-12%Cr) [15]: this is taken into account in the model in terms of, mainly, C concentration in the matrix, as will be explained later on. The density of dislocations was of the same order for all materials (~10^{13} m^{-2}); respectively: 1.2 (Fe-2.5%Cr), 5.8 (Fe-5%Cr), 6.3 (Fe-9%Cr) and 5.5 (Fe-12%Cr) ×10^{13} m^{-2} [15]. The average grain size decreased with Cr concentration; the reported values are: 50 (Fe-2.5%Cr), 35 (Fe-5%Cr), 20 (Fe-9%Cr) and 15 (Fe-12%Cr) μm [15]. For each Cr concentration we therefore used correspondingly different values of dislocation density and grain size in the simulations. The microstructure of the alloys, in terms of grain structure and dislocation density, did not change after irradiation, thereby making the parameterization of the simulation, with constant sinks, acceptable.

TEM examination reveals that, while loops with both ½⟨111⟩ and ⟨100⟩ Burgers vector appear to accumulate under irradiation at ~290°C in all Fe-Cr-C alloys, the ratio between the density of the former and the latter grows steadily with addition of Cr (from 0.66 in Fe-2.5%Cr, to 1.88 in Fe-9%Cr and 2.21 in Fe-12%Cr) [16], especially when compared to Fe-C, where 90% of the visible loops are of ⟨100⟩ type. Here we took this into account by assuming pragmatically that for all Cr concentrations all SIA clusters of any size > 4 SIA are of ½⟨111⟩ type. This assumption is translated in terms of parameters into a relatively low migration energy assigned to all these clusters (~0.1 eV) and the assumption that these clusters are efficiently trapped by C atoms and C_2V complexes, with trapping energy (E_t^{SIA}) of 0.6 and 1.3 eV, respectively [53, 54]. In Fe-C, in contrast, under irradiation at the same temperature, loops visible in TEM (i.e. > 90 SIA) were assumed to be only of ⟨100⟩ type [31], i.e. to have a higher migration energy (0.9 eV) but to be more weakly trapped by C and C_2V [53]. The attempt frequencies as a function of Cr content have been tuned as explained above. For SIA clusters < 4 SIA the migration energy values introduced in [31] are used (see Table 2).

Internal friction (IF) and magnetic after-effect (MAE) studies revealed that, as manifestation of the different initial microstructure (ferrite vs tempered martensite), C atoms were distributed differently in the investigated alloys [33]. Namely, while in the ferritic alloy (2.5 %Cr) most of the C that did not form carbides was distributed uniformly within the matrix, in the tempered martensite the matrix was virtually free of C: most of it, when not in carbides, had segregated at the martensite lath boundaries. This was arguably the most important difference and effect that the initial microstructure had on the nanostructural evolution under irradiation between the reference alloys. The C concentration in 5, 9 and 12 %Cr was accordingly set to 20 appm (significantly smaller than the C nominal content, which was in excess of 1000 appm), while for 2.5 %Cr a value of ~80 appm was chosen, based on experimental assessment [55]. What matters for our simulations is indeed the amount of C that remains in the matrix because this concentration determines the concentration of traps for point-defect clusters, as clearly explained in [31, 32]. To this regard, the only slight change with respect to Fe-C (where the amount of C in the matrix was set to 134 appm, as measured) was the choice of the

trapping energy due to C and C_2V complexes for vacancy clusters bigger than size 6: 0.35 eV instead of 0.4 eV. This fine-tuning proved to give somewhat better results and was judged to be an acceptable calibration, given that this parameter is an effective value, i.e an average value that accounts for several effects and is assumed to be independent of the size of the cluster. Finally, IF and MAE measurements also revealed that almost no free carbon atoms are left in the matrix already at 0.06 dpa in Fe-2.5% Cr, where C was observed to be in the matrix before irradiation [33]: this can be interpreted as a sign that indeed all C atoms are, already at this low dose, attached to irradiation defects (carbon-vacancy complexes and trapped loops), therefore justifying the choice of introducing from the beginning traps that act as carbon-vacancy complexes.

All simulations were performed in a non-cubic simulation box, in order to avoid potential anomalies from 1D-migrating defects entering a migration trajectory loop, due to the periodic boundary conditions which were applied in all three directions, as discussed in [56]. We used a simulation box of size 600×750×1000 a_0^3, where a_0 = 2.87×10^{-10} m is the lattice parameter of α-Fe: this box size was chosen to detect low defect densities and achieve good statistics, at the expenses of simulation time and memory, while remaining computationally doable.
A dose rate of about ~1×10^{-7} dpa/s was applied for all materials, as dictated by the flux under which the reference experiments were performed in the Mire-Cr campaign [10, 15]. In this campaign, a neutron irradiation experiment was performed in the BR2 reactor at SCK•CEN (Mol, Belgium). The materials were irradiated at ~290 °C (563 K) in a device that mimics the environmental conditions of a commercial pressurized water reactor: this irradiation temperature was therefore taken as reference for our simulations. Under these conditions, three different doses were reached during the irradiation campaign, namely 0.06, 0.6 and 1.5 dpa. Due to simulation time and memory issues, we targeted our simulation study to rationalize the results coming from the characterization of the Fe-Cr-C alloys irradiated up to 0.06 dpa and 0.6 dpa; most available microstructural characterization results are also limited to these conditions.

4. Results

4.1 Vacancy cluster density and mean size evolution compared to reference experiments

Fig. 2 represents the vacancy concentrations obtained from the OKMC simulations for the four different Fe-Cr-C model alloys analyzed in this work, as well as in Fe-C. For consistency with the experimental data, the Fe-C vacancy concentration refers to a simulation up to only 0.025 dpa, while the other points correspond to 0.06 dpa (Fe-Cr-C experimental results are from [9]; Fe-C results from [57]). Even though the simulation slightly overestimates the surviving vacancy concentration, it is evident that the trend with the addition of Cr to Fe is correct: the concentration of vacancies is approximately one order of magnitude lower in Fe-Cr-C as compared to Fe-C. The quantitative differences between simulation and experiment (e.g. the location of the minimum vacancy concentration at 2.5 %Cr in the experiment and at 5 %Cr in the simulation) should not be overemphasized, because approximations were made in the treatment of experimental PAS data to obtain the estimate of the total concentration of vacancies [9]. This introduces hardly quantifiable uncertainties.
In full agreement with our OKMC predictions, PAS experimental observations on irradiated Fe-Cr-C alloys revealed that vacancy cluster formation is either delayed in dose or even hindered if compared with Fe-C without Cr [9]. Specifically, always experimentally, the alloy containing the smallest Cr concentration (2.5 %Cr) is seen to be characterized by the presence, after 0.6 dpa, of only small vacancy clusters (2-3 vacancies, to be compared with ~10 vacancies in Fe-C irradiated to 0.2 dpa [57]), while in alloys with even higher Cr contents the average size of vacancy clusters does not exceed 1 or 2 vacancies [9]. Further elaboration of the PAS intensity data in lifetime experiments for 0.06 dpa showed clearly that the total concentration of vacancies after irradiation is drastically reduced in the presence of Cr when compared to Fe-C irradiated to half that dose, as shown in Fig. 2. Although

the vacancy concentration is then seen to increase slightly with Cr content, in absolute terms this increase remains a minor effect, possibly within experimental uncertainty.

Fig. 3 shows the simulated volume fraction of vacancies remaining in the Fe-Cr-C alloys after irradiation up to 0.06, 0.2 and 0.36 dpa, compared with the total amount of vacancies found in Fe-C at the same doses. It can be seen that the concentration of vacancies follows an increasing trend with Cr addition, which is the more pronounced the higher the dose. However, in absolute terms the concentration of vacancies in Fe-Cr-C remains always well below the concentration in Fe-C.

Together, Figs. 2 and 3 demonstrate that the reduced SIA cluster mobility leads to an increased number of recombinations (about a factor five), with correspondingly decreasing number of surviving vacancies; the smaller amount of small vacancies in turn retards the nucleation and growth of bigger vacancy clusters. Quite obviously, decreasing vacancy concentration and suppressing vacancy clustering is tantamount to hindering or delaying swelling, although of course for swelling to be measurable experimentally much higher doses need to be reached, as in [4, 6-8]. As a further proof of the link between swelling and reduced SIA cluster mobility, the model shows in Fig. 3 that, with increasing dose, the dependence of the vacancy volume fraction (i.e. void volume fraction) on Cr content takes a non-monotonic shape, which corresponds to the experimentally observed non-monotonic dependence of swelling on Cr content at high dose [7, 27] and also mirrors the non-monotonic dependence of the SIA cluster mobility reduction as a function of Cr (see Fig. 1).

To extend the picture, the vacancy cluster size distribution at 0.06 dpa obtained from the OKMC simulations for both Fe-9%Cr-C and Fe-C is compared in Fig. 4. Here, we can clearly see how the presence of Cr strongly suppresses vacancy clustering, while the concentration of mono- and di-vacancies is enhanced, in agreement with PAS experimental observations reported in [9]. However, a small queue of much bigger vacancy clusters (with number density ~10^{20} m^{-3}) is also present, which was experimentally not observed, but not looked for either: only targeted TEM analysis, not performed, may reveal (or disprove) their existence.

Finally, Fig. 5 shows the simulated vacancy cluster number density evolution with dose up to 0.6 dpa for Fe-5%Cr-C, Fe-9%Cr-C and Fe-12%Cr-C, compared with the trends obtained for Fe-C with the parameterization presented in [31]. In the figure two families of curves are shown: one corresponds to the total number density of vacancy clusters, the other to the number density of voids potentially visible in TEM (i.e. >45 vacancies, which corresponds to a size of ~1 nm). The density of voids > 1 nm is almost two orders of magnitude lower in all Fe-Cr-C alloys than the total one, which in turn is around one order of magnitude lower than in Fe-C. This difference is established since the earliest stages of the irradiation process. The number density of visible voids only in Fe-C is eventually comparable with the *total* density of vacancy clusters in the Fe-Cr-C alloys.

4.2 SIA cluster density and mean size evolution compared to reference experiments

Fig. 6 shows the number density and mean size versus dpa of TEM-visible SIA clusters (dislocation loops) up to ~0.6 dpa, as predicted by our OKMC model for all Cr concentrations, including for comparison the trend for Fe-C. TEM experimental data from both [10, 15] and [16] are also indicated. The simulations also show that both number density and mean size increase with dose in Fe-Cr-C more slowly than in Fe-C, this result being in qualitative agreement with the experimental data. However, in the simulation both number density and mean size depend somewhat more weakly on Cr content than in the experiments. This is seen in Fig. 7, where number density and mean size versus Cr content are plotted for 0.6 dpa, together with the corresponding experimental points from [10, 15] and [16].

Note that TEM characterization of the irradiated Fe-Cr-C alloys was performed on different samples (from the same irradiation) by different researchers: a first characterization was performed in [10, 15]; later, the same alloys were re-examined with a view to getting more detailed information about the type of loops and as a verification of the previous study [16]. Discrepancies exist between the results of the two studies regarding cluster mean sizes and number densities for TEM-visible SIA loops, for all Cr concentrations, especially for 0.06 dpa, the reason for which is unclear. Here we consider that the

differences are an indication of the experimental uncertainty of the results. In addition to this, the simulations results as well exhibit large scatter, in the form of oscillations, with the most plausible results lying more or less at the mid-points of the oscillations. These are due to number densities close to the minimum density detectable with the dimensions of our simulation box: an hypothetical larger box would provide richer statistics, but the computing time would be unmanageable.
However, the trends are similar in both works. The values from [10, 15] suggest at 0.6 dpa somewhat larger size and lower number density (especially for 2.5 and 5 %Cr) of visible SIA clusters than as reported in [26]. According to the latter, moreover, in Fe-9%Cr-C irradiated to 0.06 dpa TEM-visible SIA clusters were still only occasionally observed and their number was not high enough to be able to deduce a size distribution (reason for which no other alloy irradiated to that level was studied), while [10, 15] reported at the same dose average sizes of 6 nm and number densities of 1.3×10^{21} m^{-3}, and values of similar order for the other alloys. In either case, however, TEM-visible SIA cluster mean and maximum sizes, as well as density, are seen to increase with dose, although in [16] the density grows much more steeply than in [10, 15]. Also, in either case the lower Cr contents correspond to larger sizes (e.g. maximum sizes of around 60 nm were detected for 2.5 %Cr at 0.6 dpa, while for 5, 9 and 12 %Cr maximum SIA cluster sizes were found to be limited to, respectively, 44, 21 and 22 nm) [16], while the higher Cr content corresponds to lower density. Thus, one can conclude that overall the dislocation density due to visible loops decreases slightly, but steadily, with increasing Cr content.

4.3 Estimate of solute cluster density and size

We deliberately assumed that the SIA cluster population predicted by the OKMC simulations and containing between 15 and 90 SIAs might be associated with the high density of small NiSiPCr-rich solute clusters identified by APT. The leading idea is that these solutes may heterogeneously nucleate on small loops, invisible by TEM. If this assumption is plausible, then the number density of TEM-invisible loops in the simulations should be of the same order of magnitude as the number density of solute clusters found in the experiment, or somewhat smaller, because there may be solute clusters that, due to recombination, do not contain any more point-defects, or that nucleated heterogeneously elsewhere, e.g. at dislocation lines or other microstructural features. Moreover, the size of the simulated invisible loops can only be a lower bound, because it does not include the effect of the presence of solute atoms within the strain field of the loops, the effect of which will be to increase the effective size of the microstructural feature. In Fig. 8 this assumption is tested by plotting number density and mean size at 0.6 dpa of NiSiPCr-enriched clusters for the different Cr concentrations as revealed by APT [19], together with the density of invisible loops as predicted by the OKMC model, always at ~0.6 dpa. The figure shows a relatively good agreement for the density, with the loops on the lower side and, as expected, a larger discrepancy for the mean size, also with the loops on the lower side. These results make our assumption that solute clusters may nucleate on TEM-invisible loops highly plausible. For the sake of comparison the figures show also the data for Fe-C: note that the amount of invisible SIA clusters is much lower than in Fe-Cr-C alloys, as an obvious consequence of the lack of slowing down; in turn, one should consider that the decoration of invisible loops by solute atoms will likely reduce even further their mobility.
APT is the most adequate technique to look at the redistribution of solute atoms, allowing the identification of composition, size and density of solute clusters, as well as segregation at grain boundaries and dislocations, if any. APT revealed the formation under irradiation in all Fe-Cr-C alloys of solute clusters that contained, in addition to Cr atoms, also significant quantities of elements that are present only as impurities, namely Si, P and Ni [19]. Our model cannot describe solute redistribution, because solutes are simply not included in it. However, atomistic simulations have clearly shown that Cr tends to segregate on dislocation loops [59] and that other solutes follow the same trend, in particular Ni, Mn and Cu [60]. There is also unambiguous experimental evidence of segregation of Cr and other solutes (Si, Ni, Cu, …) on loops in F/M steels from energy-dispersive X-ray spectroscopy studies and also APT studies, e.g. [61] and, more recently, [62]. Furthermore, in [19] it was verified that NiSiPCr clusters observed in the Fe-Cr-C alloys examined here do have an the the

the orientation of the solute clusters was found to be compatible with the habit planes of the dislocation loops typical for bcc Fe based alloys, i.e. {111} and {110}.

5. Discussion

The parameterization developed for Fe-C systems [31, 32] proved to be both a good reference and starting point to develop a model for the nanostructural evolution under irradiation in Fe-Cr-C alloys, in a "grey alloy" approach.

In order to extend the Fe-C model to Fe-Cr-C we made three assumptions:

1. The main effect of Cr atoms in solid solution is to reduce the effective mobility of SIA-type defects (loops), without affecting either the mobility or the stability of vacancy-type clusters: the former effect has been introduced in the model on the basis of previous atomistic calculations (see Table 1 and 2, and Fig. 1).
2. Another effect of Cr is to stabilize $^1/_2\langle 111\rangle$ loops versus $\langle 100\rangle$, so we assumed all loops to be of the first type.
3. Because of the different microstructure (ferritic versus martensitic), a much smaller amount of C atoms is dispersed in the matrix in Fe-Cr-C alloys than in Fe-C.

The last one is in fact not an assumption, but a fact observed experimentally: the assumption is about the actual C concentration in the matrix, which is indicatively based on IF and MAE estimates [55], but cannot be fully precise. Introducing this difference corresponds to introducing in the model the correct initial conditions. Nonetheless, it is important to verify whether and up to what extent the difference with respect to Fe-C is due to the slowing down of SIA cluster because of Cr or to the nature of loops, or to the decrease in C content: this is discussed more in detail in what follows.

The assumption that all loops have $\frac{1}{2}\langle 111\rangle$ as Burgers vector, while being inspired to experimental observations, is a strong approximation, because, firstly, in reality $\langle 100\rangle$ loops are also present, and, secondly, the fact that loops of one or another type are observed after irradiation does not mean they were directly created as being of that type. Moreover, even though experimental evidence exists of the fact that Cr addition favours the observation of $\frac{1}{2}\langle 111\rangle$ loops [16], the precise reason is not clearly known and the determination of the ratio of the number of $\frac{1}{2}\langle 111\rangle$ to the number of $\langle 100\rangle$ loops is difficult, time consuming and affected by large uncertainty (for example, in [16] several loops could not be unambiguously recognized as belonging to either class [16]). However, to date no fully quantitative model can be proposed that would spontaneously provide the right amount of the two types of loops, not even in pure Fe. Therefore, for simplicity we assumed SIA loops of all dimensions to be of type $\frac{1}{2}\langle 111\rangle$, for all Cr contents. From the point of view of the model, as mentioned, the difference is in the mobility and in the trapping energy values to C atoms and C-vacancy complexes [31]. In order to verify how sensitive our model is to the choice of the type of SIA cluster population for the different Fe-Cr-C model alloys, we therefore also considered the opposite limiting case, i.e. we assumed that all SIA loops are of $\langle 100\rangle$ type. We observed only minor differences in the nanostructural evolution for both defect populations (vacancies and SIA) between the two limiting cases, these differences becoming visible only for the highest Cr concentrations. This result suggests, firstly, that the choice of the type of loop does not have much influence on the result, so that a more precise treatment of the two families of loops would probably not lead to significant changes in the trends; secondly, it reveals that the relative mobility of SIA clusters to each other depending on Cr content and size, and to vacancies, is more important than the absolute value assigned for the reference mobility of loops.

In order to appreciate the relative importance of the slowing down of SIA clusters due to Cr and of the lower C content in the matrix due to the different microstructure, we considered two other limiting cases. At first, we applied the parameters of Fe-C reducing the C content (i.e. the number density of traps) to 20 appm. The result is shown in Fig. 9, where the number density and the mean size evolution of, respectively, vacancy and SIA clusters are reported as a function of dose for Fe-C (no

SIA cluster slowing down due to Cr) and Fe-9%Cr-C, both with only 20 appm C. Clearly, what makes the difference between Fe-C and Fe-9%Cr-C is indeed the effect of Cr: without this effect, vacancy clustering is not suppressed, a relatively high density of visible voids forms and also the size of the SIA clusters remains large. The main effect of the reduced C content in the matrix is that the density of SIA clusters decreases (~10^{21} m^{-3} at 0.2 dpa), most likely because these are free to reach sinks where they are absorbed. The opposite case, i.e. Fe-9%Cr-C (with SIA slowing down included) with higher C content in the matrix (134 appm, as in Fe-C) is compared in Fig. 10 to the case of Fe-9%Cr-C with 20 appm C, in terms of density evolution (up to 0.06 dpa) of both vacancy and visible SIA clusters versus dose. In both cases the effect of Cr on SIA cluster mobility is included. However, the presence of a higher C content in the matrix counteracts partially the effect of Cr: vacancy clustering is not completely suppressed, the effect being limited to a reduction in the density of visible voids when compared to pure Fe. Another difference, consistent with the simulation described in the previous paragraph, is that the higher C content in the matrix leads to slightly higher density of visible loops. This suggests that, in a ferritic microstructure, where a relatively high amount of C is uniformly distributed in the matrix, as opposed to a tempered martensitic structure, where C is segregated at subgrains and lath boundaries, two effects should be visible: firstly, void formation should be enhanced; secondly, loop density should be higher. The former statement indeed corresponds to what is observed experimentally: duplex steels containing ferritic and martensitic grains show differential swelling, and the ferritic grains swell much more than the martensitic grains [63]. What just stated agrees conceptually with the fact that, for example, the TEM study performed in [16] showed that, under neutron irradiation, the loops were abundant and uniformly distributed in the mainly ferritic Fe-2.5%Cr-C, while in the other alloys, with a tempered martensite structure, loops were found almost exclusively close to dislocations and grain boundaries (this inhomogeneous distribution of loops cannot be seen in our simulations because neither grain boundaries nor dislocations are explicitly introduced in it, only their effect as sinks is).

In conclusion, the most important of the three assumptions made to introduce the effect of Cr in the simulations is clearly the first one: yet, if the C content is increased, the effect of Cr in terms of suppression of vacancy clustering is partially counteracted.
There is, however, a parameter that had to be fitted in the OKMC model in order to obtain good quantitative agreement with experiments, especially for what concerns the TEM-visible SIA cluster population number density evolution with dose: it is the ratio between the sink radius for SIA or vacancy absorption, Z (Eq. (3)). It was set to 3 in the Fe-C model [31], but a value of 1.6 had to be assumed in the case of Fe-Cr-C alloys, because otherwise, with the enhanced recombinations induced by the slowing down due to Cr, combined to efficient removal of SIAs at sinks, no loop formation was observed, while a significant density of voids appeared. On the other hand, in Fe-C the choice of Z=3 is necessary to prevent loops from starting to form at a very early stage of the irradiation process. We believe that the higher value of Z in the Fe-C model stems from the need to compensate for the assumption of immobile traps (C-vacancy complexes), which might lead to an overestimation of the number of nucleation points for SIA clusters (see discussion in [31]). In the case of irradiated Fe-Cr-C alloys, the much lower C concentration in the matrix leads to a more limited influence of the traps on the nanostructural evolution, so probably because of this a lower (and more reasonable) Z value is required. Clearly, further improvements of the model should be considered, by explicitly introducing extended sinks and/or making the effect of both C and Cr more explicit.

Despite remaining uncertainties, we believe that the present work provides, for the first time, a clear and quantitative proof of the connection between the reduction of the mobility of one-dimensionally migrating loops and the experimentally observed suppression of swelling with the addition of Cr to Fe. The non-monotonic dependence on Cr content of SIA objects mobility reduction translates into a similar dependence in the swelling suppression, here exemplified in terms of reduction of the concentration of vacancies and consequent reduced probability of vacancy clustering. At the same time, the effect of varying the C content in the matrix appears to be noteworthy. In particular, higher C content in the matrix would enhance swelling, counteracting the beneficial effect of Cr.

6. Summary and conclusions

This work represents the first approach ever to develop a physically-based model able to account for radiation-induced nanostructural changes in Fe-Cr-C systems under neutron irradiation. In our investigation an OKMC model was used to simulate a neutron irradiation experiment on Fe-Cr-C model alloys and reproduce their nanostructural evolution [9, 10, 16-19]. The inclusion of static calculations results [28-30] expressing the non-monotonic slowing down of SIA clusters due to the relatively long-ranged attractive interaction between Cr atoms and crowdions proved to be essential for our parameterization. This also represents a clear example of the application of the multiscale modelling approach: quantities calculated using atomistic models are transferred to higher scale, where the bridge is built using a suitable approximation (i.e. the splines given in Table 1).

The OKMC model successfully reproduces the SIA and vacancy cluster populations nanostructural behavior with dose at ~300°C for Fe-2.5%Cr-C, Fe-5%Cr-C, Fe-9%Cr-C and Fe-12%Cr-C model alloys. The model is also able to satisfactorily describe the formation of the NiSiPCr-enriched cluster population observed in APT, provided that they are identified with interstitial loops below the transmission electron microscope resolution.

The major influence of Cr on the nanostructural evolution of the model alloys is observed on the vacancy cluster population, whose clustering, when compared to pure Fe, appeares to be significantly suppressed already in the presence of small Cr contents. Another relevant result of this work is the prediction of a non-monotonic trend of the vacancy concentration with increasing Cr content, for any analyzed dose. This non-monotonic behavior, in fact, correlates well with the experimentally observed irradiation-induced swelling in these alloys, that is seen to first decrease and then increase with the Cr content [4, 6, 7], showing therefore the existence of a clear dependence between vacancy concentration and swelling. The ultimate explanation for the observed nanostructural evolution of the vacancy cluster population in the simulated Fe-Cr-C model alloys can be thus linked to the non-monotonic slowing down of self-interstitial atoms and SIA clusters in the presence of increasing Cr concentrations: in fact, as the mobility of the SIA objects is reduced they also become 'easier' sinks for vacancies which are therefore bound to recombine more interstitial-type defects and cluster less, therefore bringing to an overall suppression of the vacancy final concentration in the irradiated material. Moreover, in full agreement with these conclusions, a decrease of both number density and mean size of the interstitial loop population is also observed. At the same time, our study also highlightes that the beneficial effect of Cr on swelling can be counteracted by C if a large amount of it is present in the matrix.

Acknowledgments

This work has been carried out within the framework of the EUROfusion Consortium and has received partial funding from the Euratom research and training programme 2014-2018 under grant agreement No 633053. The research leading to these results was also partly funded by the Euratom's Seventh Framework Programme FP7/2007-2013 under grant agreement No. 604862 (MatISSE project) and contributes to the EERA (European Energy Research Alliance) Joint Programme on Nuclear Materials (JPNM). The views and opinions expressed herein do not necessarily reflect those of the European Commission.

Table 1

Cubic splines used to tune the SIA cluster prefactors for migration as a function of cluster size n^{SIA}. Sets of equations for all Cr contents are reported.

Cluster size (Nb of defects)	2.5%Cr	5%Cr	9%Cr	12%Cr
$n^{SIA} < 3$	$0.0112(n^{SIA})^2$-$0.1629n^{SIA}$ +0.5779	$0.0935(n^{SIA})^2$- $0.6805n^{SIA}$+1.207	$0.0112(n^{SIA})^2$- $0.1629n^{SIA}$+0.5779	$0.0200(n^{SIA})^2$- $0.2181n^{SIA}$+0.5447
$3 < n^{SIA} < 7$		-$0.0016n^{SIA}$+0.0118		
$7 < n^{SIA} < 19$	$0.0006n^{SIA}$-0.0030	$0.0001n^{SIA}$-0.0003	$0.0001(n^{SIA})^2$- $0.0008n^{SIA}$+0.0041	$0.0003(n^{SIA})^2$- $0.0043n^{SIA}$+0.0192
$19 < n^{SIA} < 37$	0.0011	$0.0002n^{SIA}$-0.0070		
$37 < n^{SIA} < 61$			$0.0007(n^{SIA})^2$-$0.0168n^{SIA}$	-$0.0004(n^{SIA})^2$+$0.0627n^{SIA}$- 1.5025
$61 < n^{SIA} < 91$	-$0.0016n^{SIA}$+0.0288			
$91 < n^{SIA} < 167$			$0.0054n^{SIA}$-0.1472	$0.0001(n^{SIA})^2$- $0.0227n^{SIA}$+1.5635
$167 < n^{SIA} < 331$				$0.0045n^{SIA}$+0.2000
$331 < n^{SIA}$	0.4487	0.7295	0.7770	0.4341

Table 2

Attempt frequencies ν of SIA clusters of sizes ≤ 7, for Fe-C [31], i.e. as from Eq. (5), and for all the investigated Fe-Cr-C alloys; the latter are given by the values for Fe-C multiplied times the diffusion coefficient ratios obtained from Table 1. Migration energies E_m for clusters ≤ 10 SIA in Fe-Cr-C are also given.

Cluster size (Nb of defects)	$\nu^{Fe\text{-}C}$ (s^{-1})	$\nu^{Fe\text{-}2.5\%Cr\text{-}C}$ (s^{-1})	$\nu^{Fe\text{-}5\%Cr\text{-}C}$ (s^{-1})	$\nu^{Fe\text{-}9\%Cr\text{-}C}$ (s^{-1})	$\nu^{Fe\text{-}12\%Cr\text{-}C}$ (s^{-1})	$E_m^{Fe\text{-}Cr\text{-}C}$ (eV)
1	$8.07\cdot10^{13}$	$3.44\cdot10^{13}$	$5.00\cdot10^{13}$	$3.44\cdot10^{13}$	$2.80\cdot10^{13}$	0.31 [50]
2	$3.41\cdot10^{14}$	$1.01\cdot10^{14}$	$7.51\cdot10^{14}$	$1.01\cdot10^{14}$	$6.44\cdot10^{13}$	0.42 [50, 51]
3	$1.18\cdot10^{13}$	$2.23\cdot10^{12}$	$8.23\cdot10^{10}$	$2.23\cdot10^{12}$	$8.27\cdot10^{11}$	0.42 [32]
4	$1.19\cdot10^{13}$	$1.26\cdot10^{12}$	$6.47\cdot10^{10}$	$1.26\cdot10^{12}$	$9.20\cdot10^{10}$	0.80 [52]
5	$1.56\cdot10^{12}$	$6.77\cdot10^{10}$	$5.97\cdot10^{9}$	$6.77\cdot10^{10}$	$7.14\cdot10^{10}$	0.10 [32]
6	$1.71\cdot10^{12}$	$6.33\cdot10^{9}$	$3.83\cdot10^{9}$	$6.33\cdot10^{9}$	$7.51\cdot10^{10}$	0.10
7	$1.71\cdot10^{12}$	$3.97\cdot10^{9}$	$1.11\cdot10^{9}$	$3.97\cdot10^{9}$	$3.42\cdot10^{9}$	0.10
8	$1.54\cdot10^{12}$	$2.50\cdot10^{9}$	$2.23\cdot10^{8}$	$1.60\cdot10^{9}$	$1.36\cdot10^{9}$	0.10
9	$1.40\cdot10^{12}$	$3.08\cdot10^{9}$	$2.69\cdot10^{8}$	$1.60\cdot10^{9}$	$1.26\cdot10^{9}$	0.10
10	$1.29\cdot10^{12}$	$3.57\cdot10^{9}$	$3.05\cdot10^{8}$	$1.73\cdot10^{9}$	$1.82\cdot10^{9}$	0.10

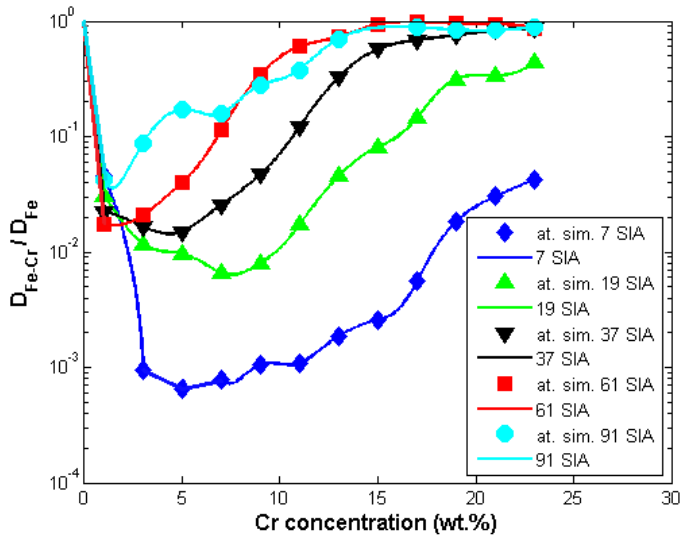

Fig. 1. Non-monotonic trend of SIA cluster diffusivity reduction, normalized to Fe-C, as a function of Cr. Atomic simulation ("at. sim.") data come from [28], while lines represent polynomial interpolations of the reference values.

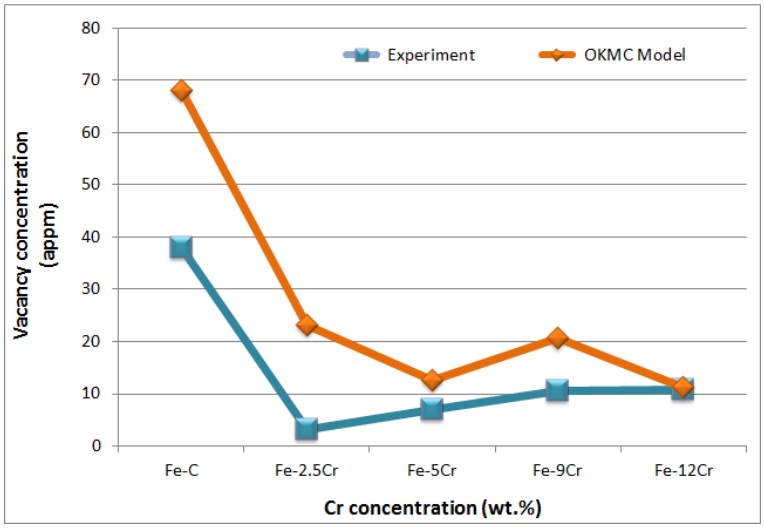

Fig. 2. Vacancy concentration, expressed in appm, at 0.06 dpa for all irradiated Fe-Cr-C alloys, compared with the total amount of vacancies in Fe-C at 0.025 dpa [31], according to the experiment [9] and OKMC simulations.

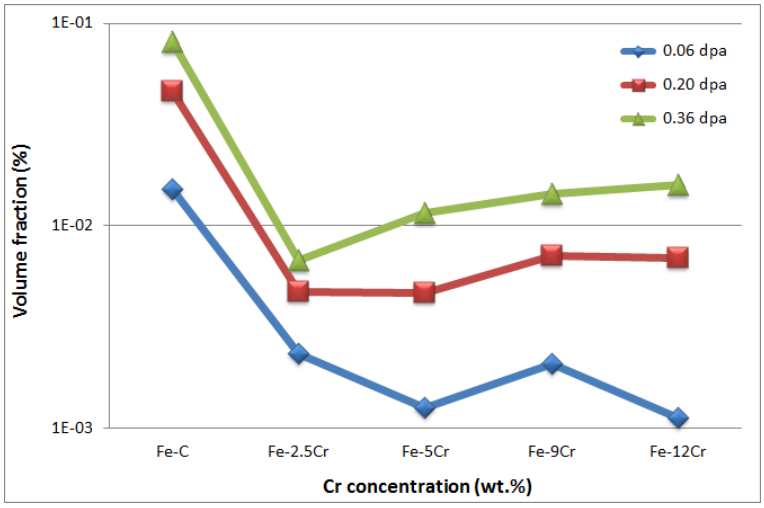

Fig. 3. Evolution of the vacancy volume fraction with Cr concentration for different irradiation doses, according to OKMC simulations; Fe-C stands for an alloys characterized by total absence of Cr.

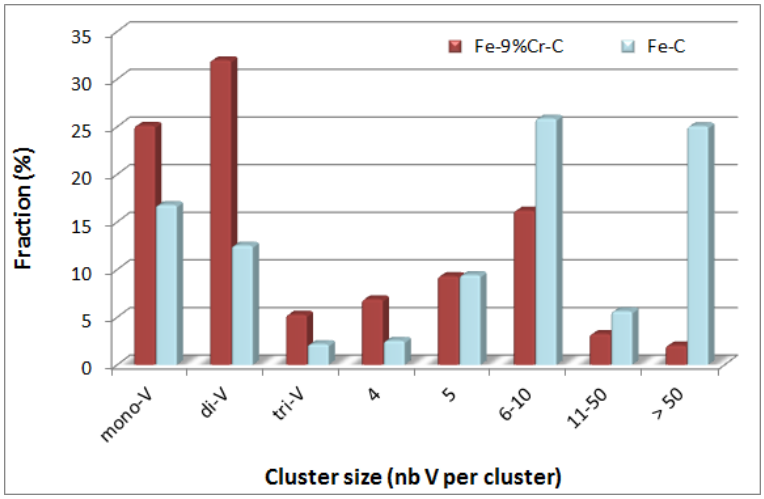

Fig. 4. Vacancy size distribution for Fe-9%Cr-C and Fe-C [31] at 0.06 dpa, as predicted by the OKMC model. The presence of Cr brings to higher concentrations of mono- and di-vacancies, while the formation of bigger clusters is hindered as compared to Fe-C.

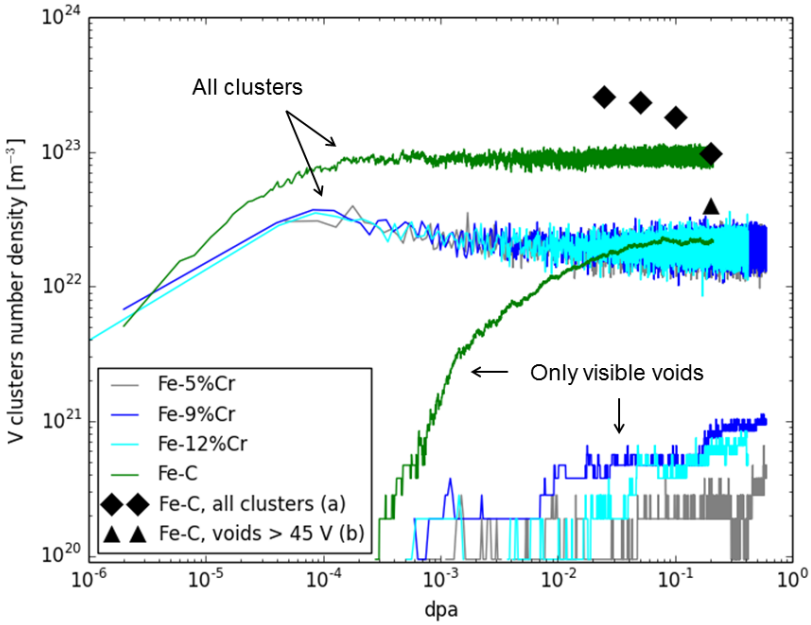

Fig. 5. Number density of vacancy clusters versus dose for 5, 9 and 12 %Cr, compared to Fe-C [31]. PAS densities are extracted by counting all clusters, assuming those ≥ 45 vacancies to have size 45, because above this size positrons do not distinguish size any more. Reference experimental points for Fe-C are also reported: (a) data from ref. [58], (b) data from ref. [39].

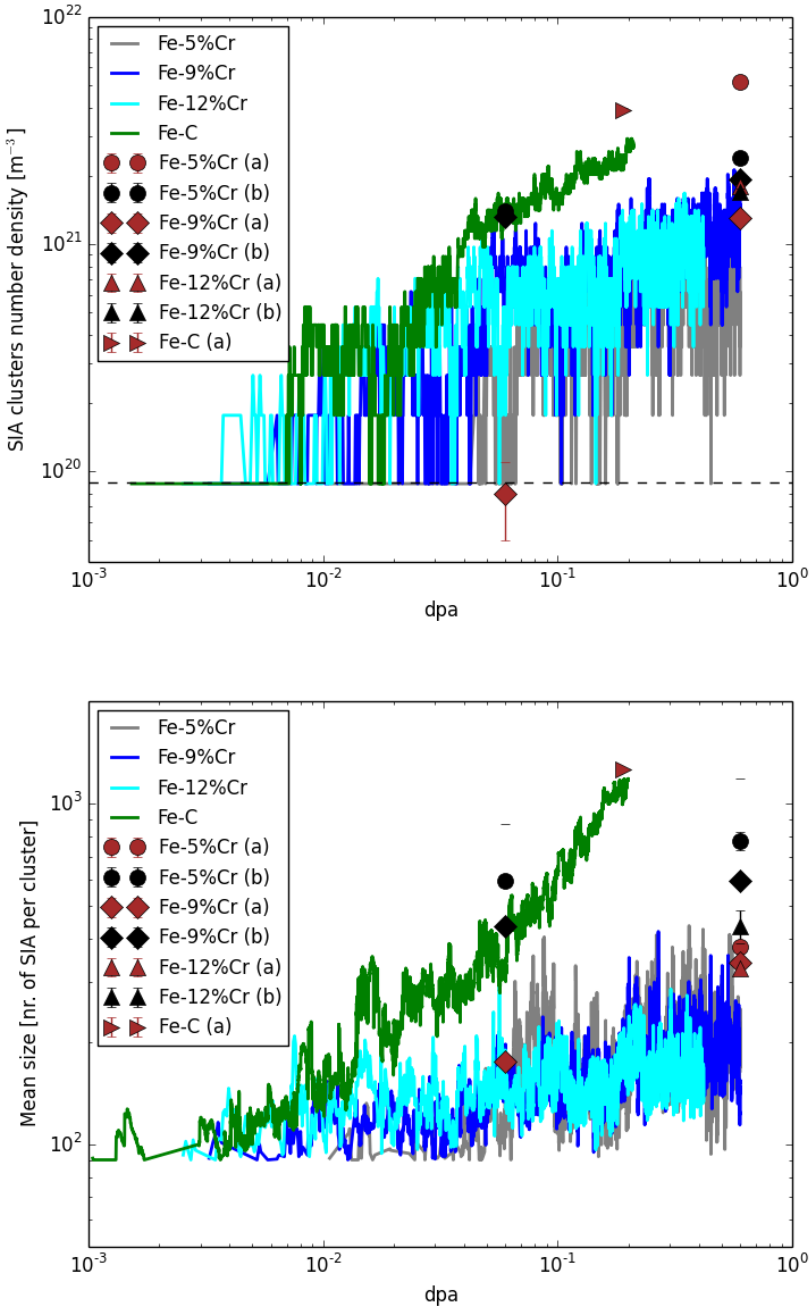

Fig. 6. TEM-visible SIA cluster number density (above) and mean size (below) evolutions versus dose for 5, 9 and 12 %Cr. Lines correspond to simulation results, dots to experimental data: (a) data from ref. [16], (b) data from ref. [10]. The dashed line represents the density corresponding to one object in the box. Loops are considered visible in TEM if their radius is larger than ~1.3 nm (90 SIA) [31]. The evolutions for TEM-visible loops in Fe-C [31] up to 0.2 dpa is also reported for comparison.

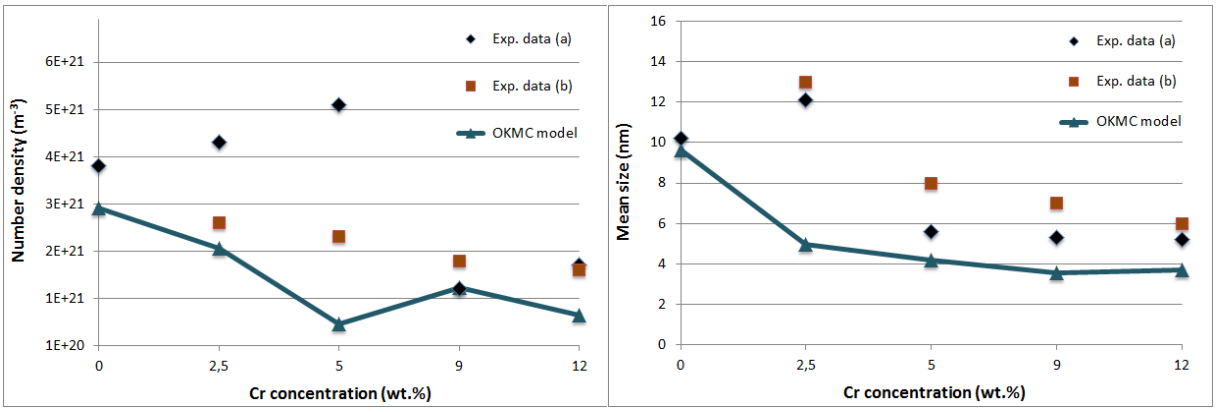

Fig. 7. Number density (left) and mean size (right) versus Cr content of TEM-visible SIA clusters at 0.6 dpa (the OKMC model result for 2.5 %Cr is given for ~0.3 dpa). The 0 %Cr x-axes value refers to pure Fe and both experimental and simulation results are given for 0.2 dpa. The experimental data (a) from [16] and (b) from [10] are also shown. Loops are considered visible in TEM if their radius is larger than ~1.3 nm (90 SIA) [31].

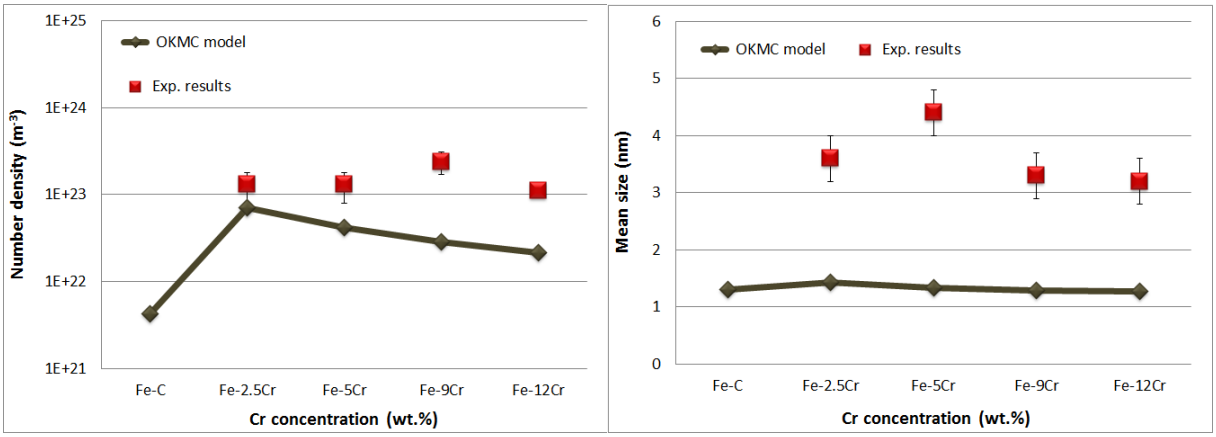

Fig. 8. Comparison between interstitial loops below TEM resolution (identified as NiSiPCr-enriched clusters) number densities (left) and mean size (right) at 0.6 dpa for different Cr content. Fe-C stands for an alloys characterized by total absence of Cr (OKMC results at 0.2 dpa). Lines correspond to simulation results, dots to experimental data as reported by APT [19]. SIA clusters between size 15 and 90 have been counted as solute clusters.

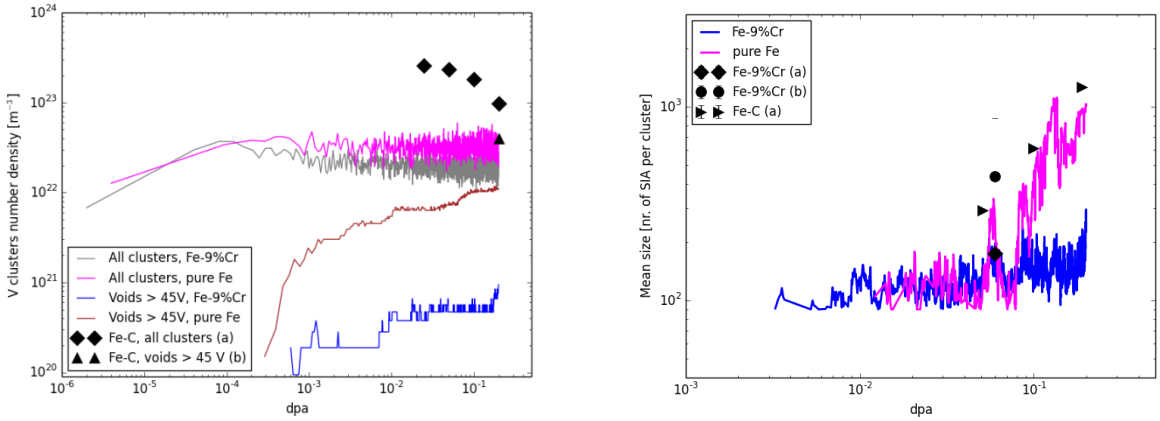

Fig. 9. Number density of vacancy clusters versus dose (left) and mean size of TEM-visible SIA (right) for Fe-9%Cr-C and pure Fe, where the C content is kept constant at 20 appm. Lines correspond to simulation results, dots to experimental data: (a) data from ref. [16], (b) data from ref. [10]. Loops are considered visible in TEM if their radius is larger than ~1.3 nm (90 SIA) [31].

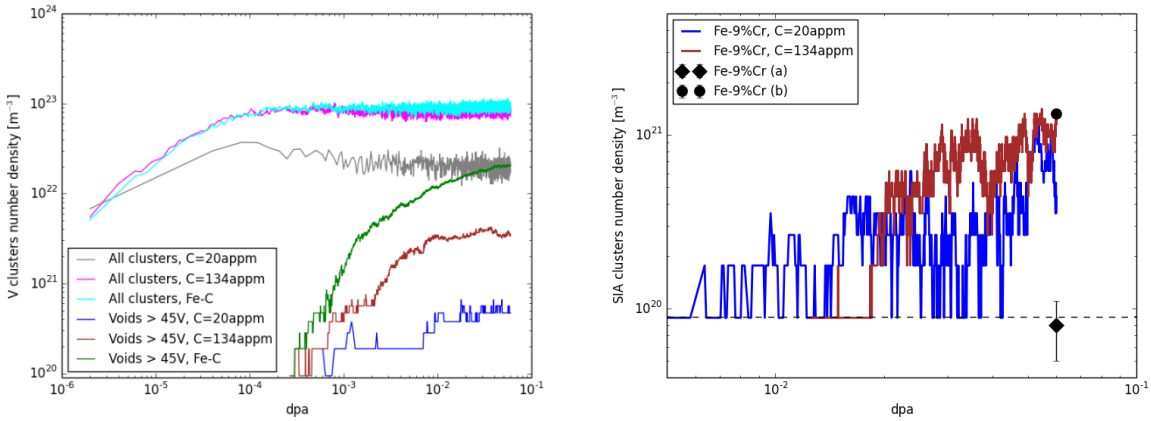

Fig. 10. Number density of vacancy clusters versus dose (left) and TEM-visible SIA (right) for Fe-9%Cr with different C contents (20 appm and 134 appm). The evolution for vacancy clusters in Fe-C [31] is also reported for comparison. The dashed line represents the density corresponding to one object in the box. Loops are considered visible in TEM if their radius is larger than ~1.3 nm (90 SIA) [31].

Acknowledgments

This work has been carried out within the framework of the EUROfusion Consortium and has received funding from the Euratom research and training programme 2014-2018 under grant agreement No 633053. It was also partially funded by the Euratom's Seventh Framework Programme FP7/2007-2013, under grant agreement No. 604862 (MatISSE project) and contributes to the EERA (European Energy Research Alliance) Joint Programme on Nuclear Materials. The views and opinions expressed herein do not necessarily reflect those of the European Commission.

References

[1] H. Tanigawa, K. Shiba, A. Moeslang, R.E. Stoller, R. Lindau, M.A. Sokolov, G.R. Odette, R.J. Kurtz, S. Jitsukawa, Journal of Nuclear Materials 417 (2011) 9.

[2] T.R. Allen, J.T. Busby, R.L. Klueh, S.A. Maloy, M.B. Toloczko, JOM 60 (2008) 15.

[3] Yeong-il Kim, Yong Bum Lee, Chan Bock Lee, Jinwook Chang, and Chiwoong Choi, Science and Technology of Nuclear Installations 2013 (2013) 290362 (18 pages). http://dx.doi.org/10.1155/2013/290362

[4] E.A. Little, D.A. Stow, Journal of Nuclear Materials 87 (1979) 25-39.

[5] D.S. Gelles, Journal of Nuclear Materials 108&109 (1982) 515.

[6] S. Porollo, A. Dvoriashin, A. Vorobyev, Y. Konobeev, Journal of Nuclear Materials 256 (1998) 247-253.

[7] F.A. Garner, M.B. Toloczko, B.H. Sencer, Journal of Nuclear Materials 276 (2000) 123-142.

[8] Y. Konobeev, A. Dvoriashin, S. Porollo, F. Garner, Journal of Nuclear Materials 355 (2006) 124.

[9] M. Lambrecht, L. Malerba, Acta Materialia 59 (2011) 6547-6555.

[10] M. Matijasevic, A. Almazouzi, Journal of Nuclear Materials 377 (2008) 147-154.

[11] K. Arakawa, M. Hatanaka, H. Mori, K. Ono, Journal of Nuclear Materials 329-333 (2004) 1194.

[12] M. Hernandez-Mayoral, Z. Yao, M.L. Jenkins, M.A. Kirk, Philosophical Magazine 88 (2008) 2881

[13] Z. Yao, M. Hernandez-Mayoral, M.L. Jenkins, M.A. Kirk, Philosophical Magazine 88 (2008) 2851.

[14] M.L. Jenkins, Z. Yao, M. Hernandez-Mayoral, M.A. Kirk, Journal of Nuclear Materials 389 (2009) 197.

[15] M. Matijasevic, Ph.D.thesis, University of Ghent, 2007.

[16] M. Hernández-Mayoral, C. Heintze, E. Oñorbe, Submitted to Journal of Nuclear Materials (2014).

[17] C. Heintze, A. Ulbricht, F. Bergner, H. Eckerlebe, Journal of Physics: Conference Series 247 (2010) 012035.

[18] A. Ulbricht, C. Heintze, F. Bergner, H. Eckerlebe, Journal of Nuclear Materials 407 (2010) 29.

[19] V. Kuksenko, C. Pareige, P. Pareige, Journal of Nuclear Materials 432 (2013) 160.

[20] C.D.Hardie, C.A.Williams, S. Xu, S.G.Roberts, Journal of Nuclear Materials 439 (2013) 33-40.

[21] L. Malerba, A. Caro, J. Wallenius, Journal of Nuclear Materials 382 (2008) 112.

[22] D. Terentyev, G. Bonny, N. Castin, C. Domain, L. Malerba, P. Olsson, V. Moloddtsov, R.C. Pasianot, Journal of Nuclear Materials 409 (2011) 167.

[23] C. Fazio, D.G. Briceño, M. Rieth, A. Gessi, J. Henry, L. Malerba, Nuclear Engineering and Design 241 (2011) 3514.

[24] L. Malerba, G. Bonny, D. Terentyev, E.E. Zhurkin, M. Hou, K. Vortler, K. Nordlund, Journal of Nuclear Materials 442 (2013) 486.

[25] D. Terentyev, G. Bonny, C. Domain, G. Monnet, L. Malerba, Journal of Nuclear Materials 442 (2013) 470.

[26] D. Terentyev, P. Olsson, L. Malerba, Journal of Nuclear Materials 386-388 (2009) 140-142.

[27] D. Terentyev, L. Malerba, A. V. Barashev, Philosophical Magazine Letters, Vol. 85 (2005) 587-594.

[28] D. Terentyev, P. Olsson, L. Malerba, A.V. Barashev, Journal of Nuclear Materials 362 (2007) 167-173.

[29] D. Terentyev, L. Malerba, A. Barashev, Philosophical Magazine 88 (2008) 21.

[30] D. Terentyev, M. Klimenkov, L. Malerba, Journal of Nuclear Materials 393 (2009) 30-35.

[31] V. Jansson, M. Chiapetto, L. Malerba, Journal of Naclear Materials 442 (2013) 341-349.

[32] V. Jansson, L. Malerba, Journal of Nuclear Materials 443 (2013) 274-285.

[33] M. Hernández Mayoral et al., Deliverable D4.9 (Public), GETMAT Project, Grant Agreement N°: FP7-2121175 (2013).

[34] C. Domain, C. Becquart, L. Malerba, Journal of Nuclear Materials 335 (2004) 121-145.

[35] A. B. Bortz, M. H. Kalos, and J. L. Lebowitz, Journal of Computational Physics 17, 10 (1975).

[36] W. Young, E. Elcock, Proceedings of the Physical Society 89 (1966) 735.

[37] A.B. Bortz, M.H. Kalos, J.L. Lebowitz, Journal of Computational Physics 17 (1975) 10-18.

[38] F. Nichols, Journal of Nuclear Materials 75 (1978) 32-41.

[39] M. Hernández-Mayoral, D. Gómez-Briceño, Journal of Naclear Materials 399 (2010) 146-153.

[40] C. Domain, C. Becquart, L. Malerba, in: N. Ghoniem (Ed.), Proceedings of Second International Conference on Multiscale Materials Modeling: October 11 - 15, 2004, Los Angeles, California, Mechanical and Aerospace Engineering Department, University of Calif., 2004.

[41] R. Stoller, Journal of Nuclear Materials 233 (1996) 999–1003.

[42] R. Stoller, G. Odette, B.Wirth, Journal of Nuclear Materials 251 (1997) 49–60.

[43] R. Stoller, A. Calder, Journal of Nuclear Materials 283 (2000) 746–752.

[44] M. Norgett, et al., Nuclear Engineering and Design 33 (1975) 50–54.

[45] P. Olsson, T.P.C. Klaver, C. Domain, Physical Review B 81 (2010) 054102.

[46] E. del Rio, J.M. Sampedro, H. Dogo, M.J. Caturla, M. Caro, A. Caro, J.M. Perlado, Journal of Nuclear Materials 408 (2011) 18.

[47] A. Barashev, S. Golubov, H. Trinkaus, Philosophical Magazine A 81 (2001) 2515–2532.

[48] B. Wirth, G. Odette, D. Maroudas, G. Lucas, Journal of Nuclear Materials 276 (2000) 33–40.

[49] K. Arakawa, K. Ono, M. Isshiki, K. Mimura, M. Uchikoshi, H. Mori, Science 318 (2007) 956.

[50] S. Takaki, J. Fuss, H. Kuglers, U. Dedek, H. Schultz, Radiation Effects and Defects in Solids 79 (1983) 87-122.

[51] C. Fu, F. Willaime, P. Ordejón, Physical Review Letters 92 (2004) 175503.

[52] Y. Fan, A. Kushima, B. Yildiz, Physical Review B 81 (2010) 104102.

[53] N. Anento, A. Serra, Journal of Nuclear Materials 440 (2013) 236.

[54] D. Terentyev, N. Anento, A. Serra, V. Jansson, H. Khater, G. Bonny, Journal of Nuclear Materials 408 (2011) 272.

[55] B. Minov, private communication.

[56] L. Malerba, C. Becquart, C. Domain, Journal of Nuclear Materials 360 (2007) 159.

[57] M. Lambrecht, A. Almazouzi, Journal of Nuclear Materials 385 (2009) 334.

[58] M. Lambrecht, E. Meslin, L. Malerba, M. Hernandez-Mayoral, F. Bergner, P. Pareige, B. Radiguet, A. Almazouzi, Journal of Nuclear Materials 406 (2010) 84.

[59] E.E. Zhurkin, D. Terentyev, M. Hou, L. Malerba, G. Bonny, Journal of Nuclear Materials 417 (2011) 1082.

[60] G. Bonny, D. Terentyev, E.E. Zhurkin, L. Malerba, Journal of Nuclear Materials 452 (2014) 486.

[61] I.M. Neklyudov, V.N. Voyevodin, Journal of Nuclear Materials 212 (1994) 39.

[62] Z. Jiao, G.S. Was, Acta Materialia 59 (2011) 4467.

[63] V. Bryk, O. Borodin, A. Kalchenko, V. Voyevodin, V. Ageev, A. Nikitina, V. Novikov, V. Inozemtsev, A. Zeman, and F. Garner, "Ion issues on irradiation behaviour of structural materials at high doses and gas concentrations", Proceedings 11th International Topical Meeting on Nuclear Applications of Accelerators (AccApp Conference, 2013), 5-8 August, 2013, Bruges, Belgium; available at http://fullpapers.flexmax.eu/accapp2013/protected/MOOMA08.pdf.